Nonlinear Electromagnetic Time Reversal in an Open Semireverberant System

Sun K. Hong,[1][*] Victor M. Mendez,[1] Trystan Koch,[2,3] Walter S. Wall,[1] and Steven M. Anlage[2]

[1]*Tactical Electronic Warfare Division, Naval Research Laboratory, Washington, D.C. 20375, USA*
[2]*Department of Physics, University of Maryland, College Park, Maryland 20742, USA*
[3]*Envisioneering, Inc., Alexandria, Virginia 22303, USA*

We consider nonlinear electromagnetic time reversal (TR) applied to a semireverberant complex enclosure containing a discrete passive nonlinear circuit. Unlike closed reverberant systems used for the previous demonstrations of nonlinear electromagnetic TR, the experimental system used here better represents realistic environments that are often far more lossy. Moreover, we demonstrate the use of pulse inversion to extract nonlinear responses for electromagnetic time reversal, which could help overcome potential practical-implementation issues. Concentrating on the application of this technique as an efficient power-delivery method, we evaluate the peak power enhancement resulting from TR focusing at the location of the nonlinear circuit.

I. INTRODUCTION

The concept of a time-reversal mirror (TRM) has been studied and demonstrated extensively as a means of focusing acoustic or electromagnetic waves both spatially and temporally [1–6]. In principle, a TRM exploits the time-reversal symmetry in the lossless wave equation, where there exist both time-forward and time-reversed solutions to a wave traveling in a particular direction. An ideal TRM would enclose a medium in which a localized source emits a waveform. The TRM captures all of the waves that originated from the source at every point on the enclosing surface. The captured waveform is then time reversed and transmitted back into the medium, such that the resulting waves will converge back to the source in both time and space, thus reconstructing a time-reversed version of the original waveform at the source.

Practical TRMs are realized by employing an array of antennas (or transducers) that receive and transmit waveforms. An array provides the spatial coverage needed to capture a significant portion of the waves emitted from a source. Furthermore, complex scattering media are shown to enhance the performance of a TRM due to an effective increase in spatial coverage by capturing parts of the waves redirected by scattering [7]. TRMs are studied for both acoustic and electromagnetic waves in various applications such as underwater communications [8–10], sensors [11–13], wireless communications [4,14–18], imaging [19–22], radars [23,24], and beam forming [25–28].

Of particular interest here is an electromagnetic TRM in a closed wave-chaotic environment that exhibits a strong reverberant condition [6,13,29]. In such an environment, a

TRM can be simplified to a single-antenna configuration when a short pulse is used as the original waveform. That is, when a pulse is transmitted from a source, all of the multipath rays, in principle, will eventually intersect with the TRM, assuming a lossless medium and boundaries. This intersection allows for the TRM to capture all of the waves that originated from the source. Even with the loss at boundaries and a finite recording time in an experimental system, a good TR reconstruction can be achieved with a single-antenna TRM in a wave-chaotic system [6]. TRMs in this manner are demonstrated for indoor wireless communications [4,18] and sensors [29].

As indicated above, a TRM requires the response of a system to an initial short pulse from a source, hereafter referred to as the channel response. However, in order to employ a TRM in a broader range of applications, it is desirable to obtain the channel response without physically sending a short pulse from the source location. To this end, a recent demonstration with a single-antenna electromagnetic TRM in a closed wave-chaotic system has shown that the reconstruction of a short pulse can be achieved when a localized nonlinearity is enclosed in the system [30]. That is, when a short pulse enters the system, its interaction with the nonlinear element generates harmonics, and the element becomes a new source originating from the location of the nonlinear element. When the radiated nonlinear excitation is captured by the TRM, time reversed and retransmitted, the reconstruction of the original nonlinear excitation will take place at the location of the nonlinear element. This nonlinear electromagnetic time reversal is demonstrated for secure wireless communications [30] and could also be used for wireless power transfer. This nonlinear time reversal (NLTR) has been previously demonstrated in acoustics [31–33] and also in optics [34] for various applications such as imaging nonlinear scatterers [32], sensing defects in materials [33], and biomedical therapy [34].

[*]Corresponding author.
sun.hong@nrl.navy.mil

Previous work has successfully demonstrated electromagnetic NLTR with a discrete nonlinear device in a closed, reverberant cavity [30], which provides good conditions for a basic demonstration of the concept. For most realistic applications, however, the scattering environment will be far less reverberant, with openings and windows greatly reducing the number of multipath rays. Furthermore, the signal level of harmonic responses would be lower by orders of magnitude than that of the fundamental response, which could be a challenge in linearity or dynamic-range-limited digital receivers. Also, any overlap between the spectrum of the fundamental and harmonic frequencies will limit the isolation of the harmonic responses when a bandpass filter around the harmonic frequencies is applied as in Ref. [30].

In this paper, we investigate electromagnetic NLTR, addressing the aforementioned practical issues. Here we use an experimental system consisting of an open complex enclosure with many apertures to better represent a realistic environment. To overcome the issues of receiver linearity and harmonic isolation, we propose to use pulse inversion [35], which will suppress fundamental and odd-order harmonics while enhancing even-order harmonic responses. We show that the reconstruction of the original nonlinear excitation does occur at the location of the nonlinear element when pulse inversion is applied to extract harmonic responses. Furthermore, we introduce a simple but practical method of evaluating the performance of NLTR by comparing the peak power at the nonlinear element resulting from time-reversal focusing and the peak power at the same location due to the transmission of simple, nondispersed pulses without time reversal. This performance metric will be particularly useful for evaluating NLTR's capability to efficiently deliver short electromagnetic pulses to a localized nonlinear element in a complex propagation environment in applications such as wireless power transfer, directed energy, and biomedical applications.

II. EXPERIMENT

A. Experimental setup

An experimental system consisting of a partially open wave-chaotic metallic enclosure as shown in Fig. 1 is constructed. The dimensions of the enclosure are $1.21 \text{ m} \times 1.27 \text{ m} \times 0.65 \text{ m}$ ($W \times D \times H$). See the Supplemental Material [36] for the comparison of loss between this open cavity and a closed cavity. As shown in the figure, windows are placed across the front wall and halfway across the side walls. The height of the windows is 0.32 m. A mode-mixing paddle is located inside the enclosure towards the left back wall. A wideband monoconical antenna loaded with a passive nonlinear circuit is placed inside the cavity. The nonlinear circuit element is represented by Mini-Circuits passive-frequency doublers
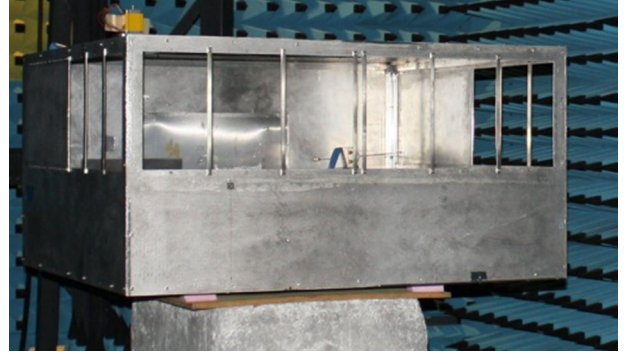
FIG. 1. Metallic enclosure used for the nonlinear time-reversal experiment in an anechoic chamber. The nonlinear element is placed inside the enclosure while transmit and receive (TRM) antennas are placed outside the enclosure.

(three different models are used for different frequencies [37]). The input and output of the frequency doubler are connected to the antenna feed via a power divider, such that the nonlinear excitation would be reradiated into the enclosure through the same port. Two external ports, namely, port 1 and port 2 (TRM port), consist of ultrawideband dual-ridged horn antennas and are placed in a bistatic configuration with the spacing of 1.6 m at a distance of 1.5 m from the front center of the enclosure for both ports.

As illustrated in Fig. 2, the experiment consists of two distinct stages: the interrogation (time forward) and focusing (time reversed). In the interrogation stage [Fig. 2(a)], a 10-ns microwave pulse with a carrier frequency of f_0 (three different f_0's are used throughout the experiment) is transmitted into the enclosure from port 1. The pulse is generated directly from a Tektronix AWG70002 arbitrary waveform generator. As the pulse propagates around the enclosure, it enters the nonlinear port, exciting the nonlinear circuit element. The nonlinear excitation is then reradiated into the enclosure. The signal that port 2 receives is a combination of the scattering of the original pulse and the nonlinear excitation. From this combined response, the nonlinear response is extracted (by using pulse inversion discussed in the next subsection) and time reversed in the postprocessing. In the focusing stage [Fig. 2(b)], the time-reversed nonlinear response is retransmitted into the enclosure from port 2. Since the signal contains only the effective channel response from the nonlinear port, the waves converge exclusively at the nonlinear port, thereby reconstructing the original nonlinear excitation. In this stage, the nonlinear circuit and power divider are removed in order to monitor the reconstruction.

B. Nonlinear response extraction using pulse inversion

For a single-carrier interrogation pulse at f_0, the resulting nonlinear responses occur at harmonic frequencies, which can be extracted by using a bandpass filter, say, at
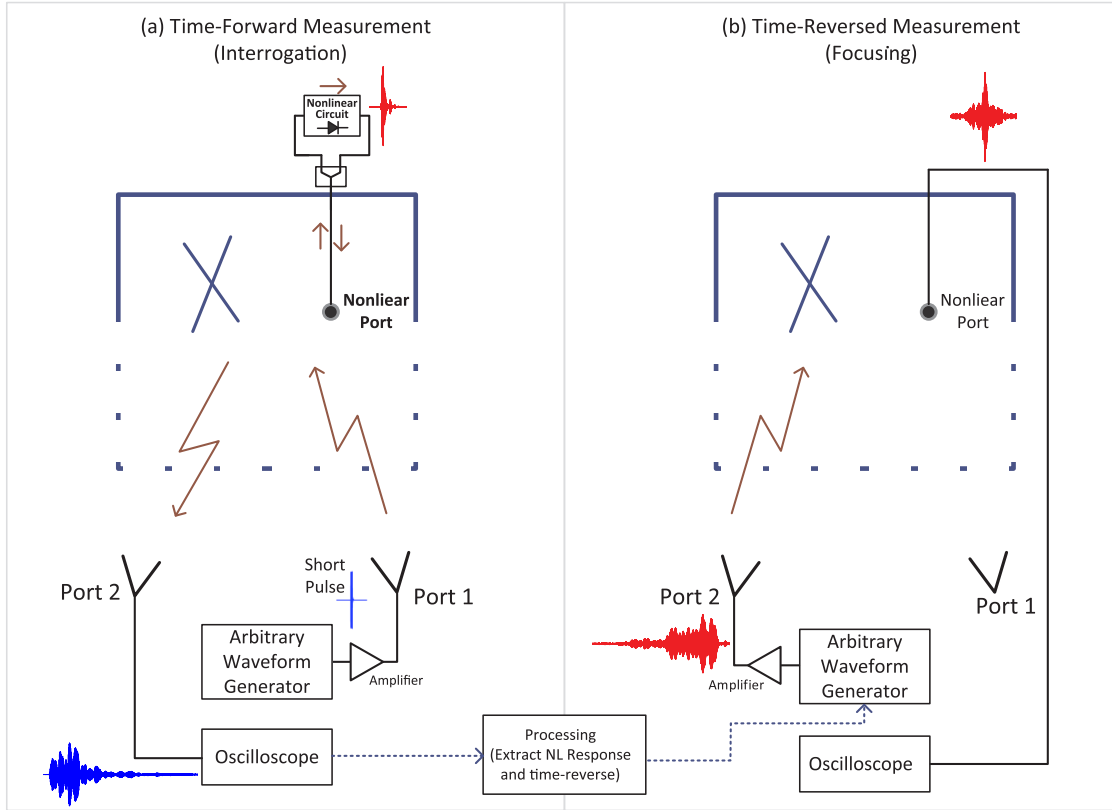
FIG. 2. Nonlinear time-reversal experimental setup. (a) Time-forward or interrogation stage, where a short pulse is transmitted from port 1 to excite nonlinearity and the total response is received by port 2. (b) Time-reversed or focusing stage, where the nonlinear response is extracted, time reversed, and retransmitted from port 2 into the enclosure. Time-reversal reconstruction of the nonlinear excitation is monitored at the nonlinear port.

$2f_0$. However, it becomes a challenge in more arbitrary cases, especially when there is a significant overlap in the spectrum around fundamental and harmonic frequencies due to a short, wideband interrogation pulse. Furthermore, the power level of the nonlinear excitation tends to be significantly lower than that of the linear response, which may limit the reception of the nonlinear response due to the linearity or dynamic-range limit in a digital receiver. Such potential issues can be overcome via pulse inversion [35], which is applied extensively in contrast-enhanced ultrasound imaging [38].

Here we apply pulse inversion to our nonlinear time-reversal experiment for extracting nonlinear responses. Consider two interrogation pulses, namely, $p^+(t)$ and $p^-(t)$, such that $p^-(t) = -p^+(t)$. When either of these pulses is transmitted into the enclosure from port 1, the resulting channel response received by port 2 is

$$c_{21}(t) = c_{21L}(t) + c_{21NL}(t), \qquad (1)$$

where the first and second terms represent the linear and nonlinear responses, respectively. The linear response, which is from the scattering of the original pulse, is

$$c_{21L}(t) = Ap(t) \circ h_{21}(t), \qquad (2)$$

where $\circ$ denotes temporal convolution, $p(t)$ is an interrogation pulse, A is a scalar constant representing the transmit amplitude (from an amplifier), and

$$h_{21}(t) = \sum_{n=1}^{\infty} a_n \delta(t - \tau_n), \qquad (3)$$

representing the impulse response between port 1 and port 2 as a weighted sum of ray trajectories between the two ports. The nonlinear response in Eq. (1) is

$$c_{21NL}(t) = g(t) \circ h_{2,NL}(t), \qquad (4)$$

where $h_{2,NL}(t)$ is the impulse response between the non-linear port and port 2, which can also be represented as a sum of ray trajectories similar to Eq. (3), and $g(t)$ is the signal excited (output) at the nonlinear port represented in terms of a power-series expansion as

$$g(t) = \sum_{k=1}^{\infty} b_k e^k(t), \qquad (5)$$

assuming memoryless nonlinearity. The incident signal at the nonlinear port, $e(t)$, is represented as

$$e(t) = A p(t) \circ h_{\mathrm{NL},1}(t), \qquad (6)$$

where

$$h_{\mathrm{NL},1}(t) = \sum_{m=1}^{\infty} c_m \delta(t - \tau_m), \qquad (7)$$

which is also a weighted sum of ray trajectories between the nonlinear port and port 1. This result suggests that, in general, $g(t)$ is not a single pulse but rather a set of many pulses as a result of multiple paths (multipath) from port 1 to the nonlinear port. However, we observe that $g(t)$ is fairly well localized in time in the form of a single or a set of a few short pulses [as shown, for example, in Fig. 3(b)].
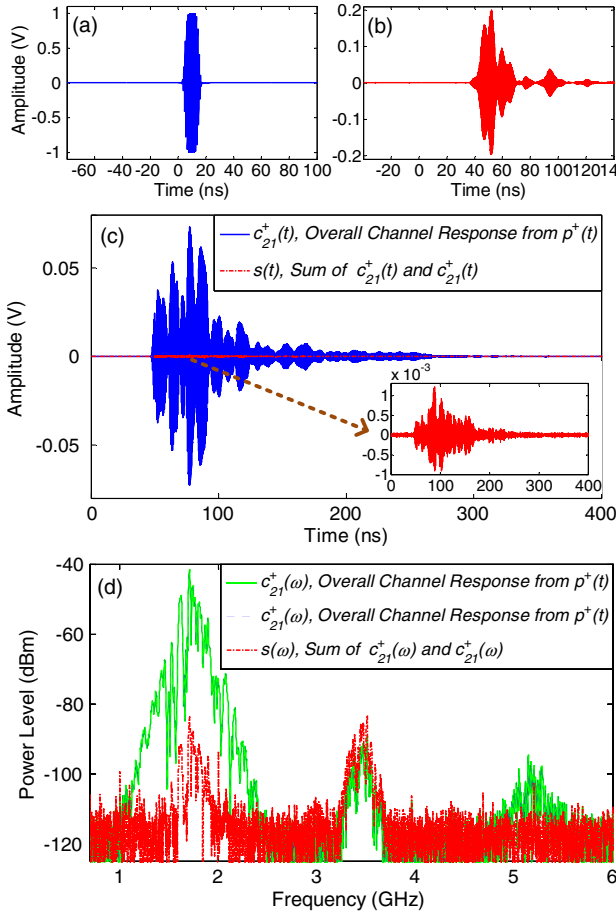
FIG. 3. Experimental signals in the interrogation stage. (a) Original 10-ns interrogation pulse ($f_0 = 1.75$ GHz). (b) Excited signal (output) at the nonlinear port. (c) Overall channel response from the positive interrogation pulse (blue) and the signal after summing the inverted channel responses (red and inset). (d) Spectrum of overall channel responses from the positive (green) and negative (blue) interrogation pulses and the signal after summing the inverted channel responses (red). The even-order harmonic signal is extracted due to the suppression of the fundamental and odd-order harmonic.

This observation is primarily due to the nonlinear relationship between the input and output signals at the nonlinear port, where only the strongest input pulses will generate significant output. This relationship means that the early trajectories (direct path and short orbits) containing the largest weights (c_m) produce most of the harmonic content, thereby allowing the resulting $g(t)$ to be rather localized in time. A similar observation has been made even in a highly reverberant closed cavity [30], although $g(t)$ is spread out more in time in that case due to ray trajectories with larger weights in later time. Note that, while we limit our demonstration to an open, semireverberant system which represents a more realistic environment, the equations derived here represent general phenomena in any reverberant system containing a multipath.

By applying the two inverted pulses separately, the channel response in Eq. (1) becomes

$$c_{21}^{+}(t) = c_{21L}^{+}(t) + c_{21\mathrm{NL}}^{+}(t), \quad c_{21}^{-}(t) = c_{21L}^{-}(t) + c_{21\mathrm{NL}}^{-}(t). \qquad (8)$$

By summing these two responses, we get

$$s(t) = g_e(t) \circ h_{2,\mathrm{NL}}(t), \qquad (9)$$

where the linear term is eliminated and

$$g_e(t) = \left[\sum_{k=1}^{\infty} 2 b_{2k-1} e^{2k-1}(t) \right]. \qquad (10)$$

Note that only the even-order nonlinear terms remain (enhanced by a factor of 2), indicating that $s(t)$ now represents a channel response between the nonlinear port and port 2. When $s(t)$ is time reversed and retransmitted into the enclosure, the resulting signal at the nonlinear port is

$$r(t) = B g_e(-t) \circ [h_{2,\mathrm{NL}}(-t) \circ h_{2,\mathrm{NL}}(t)], \qquad (11)$$

which is an approximate reconstruction of the even-order nonlinear excitation (time-reversed version) as the term on the right represents an autocorrelation that approaches the Dirac δ function in the limit of zero cavity loss. Here, B is a scalar constant representing the transmit amplitude from an amplifier. Notice that the odd-order nonlinear terms are eliminated from pulse-inversion excitation.

The reconstruction of the nonlinear excitation results from the focusing of waves in both time and space. Although the equations shown here are only as a function of time, we can relate them to spatial focusing by considering the signals that would be measured if probes were placed at locations other than that of the nonlinear port. That is,

$$n(t) = B g_e(-t) \circ [h_{2,\mathrm{NL}}(-t) \circ h_{23}(t)], \qquad (12)$$

where $h_{23}(t)$ represents the impulse response between port 2 and a third probe placed at any location other than that of the nonlinear port in the enclosure. In this case, $h_{23}(t)$ differs from $h_{2,\mathrm{NL}}(t)$ and the correlation is low between the two, which means that the waves do not interfere coherently. Although we consider only $r(t)$ in the experimental results in Sec. III, we demonstrate the spatial focusing in the Supplemental Material [36], where a two-dimensional model is simulated to obtain $r(t)$ and $n(t)$ at various locations.

III. RESULTS AND DISCUSSION

Measurements from the setup shown in Fig. 2 are taken by using a 10-ns single-tone interrogation pulse at three different carrier frequencies (f_0), namely, 1, 1.75, and 3.5 GHz, which represent three different electrical sizes of the enclosure. An amplifier at port 1 produces 30 dBm of peak power in the interrogation pulse. At each frequency, several different enclosure configurations are realized by rotating the mode-mixing paddle to change the scattering condition in the enclosure. In Fig. 3, an example of the signals in the interrogation stage ($f_0 = 1.75$ GHz) is presented. In Fig. 3(a), an original 10-ns interrogation pulse, $p^+(t)$, is shown. Figure 3(b) displays the excitation at the nonlinear port, $g(t)$, which is probed at the output of the nonlinear circuit. It shows that the nonlinear excitation in this case is a set of a few pulses with the most weight (highest amplitude) in the first pulses. As discussed earlier, many of the nonlinear excitations in the experiment consist of a similar form, i.e., consisting of a single to few pulses.

In Fig. 3(c), the overall channel response due to a positive interrogation pulse, $c_{21}^+(t)$, is plotted in comparison with the sum of the inverted channel responses, $s(t)$, which represents the extracted nonlinear response. The channel response is spread over a few hundred nanoseconds due to the multipath scattering in the enclosure. Also, it is clear that the nonlinear response is significantly lower in amplitude than the linear response. As shown in the spectrum [Fig. 3(d)], the amplitude around f_0 is over 40 dB higher than that of the nonlinear response at $2f_0$ and $3f_0$. On the other hand, in the sum signal a significant suppression of amplitude around f_0 and $3f_0$ can be observed, while there is an increase (approximately 6 dB) around $2f_0$, which is consistent with Eq. (9). Notice that the energy around f_0 is not completely suppressed. This result is primarily due to the limitation in the alignment and sampling of the two inverted pulses. Further suppression could be achieved by minimizing the error between the two inverted pulses. However, it is clear in the plot that the magnitude of the suppression is near 50 dB, which is significant enough to reduce the level of the linear response below the nonlinear response. This result suggests that if pulse inversion were to be implemented in hardware (by using delay lines and combiners) before the receiver, it could resolve potential receiver linearity issues and help

detect very small harmonic responses in the presence of a large fundamental response. Additional processing such as high-pass filters could be used for further suppression when there is minimal spectral overlap between the linear and nonlinear responses as in the case of this experiment.

In Fig. 4(a), the signal reconstructed at the nonlinear port, $r(t)$, obtained in the focusing stage by transmitting the time-reversed $s(t)$ from Fig. 3(c) is shown in comparison with the original excitation at the nonlinear port plotted time reversed for better comparison. Although there are time sidelobes in the reconstructed signal due to the less-than-ideal TRM and loss in the system, the reconstructed signal resembles the original excitation, particularly around 375 ns, where the reconstruction of the main peaks takes place. Similar results are obtained throughout other runs in the experiment with different configurations and frequencies.

Here we discuss the aspect of time reversal as a means of efficiently concentrating peak power at a given location, which in this case is a nonlinear port. In this regard, we consider the enhancement in peak amplitude of the signal delivered to the nonlinear port by using time reversal compared to when nondispersed, simple microwave pulses are used. To this end, we define a parameter, hereafter referred to as the peak gain, as

$$\mathrm{PG} = 10\log\left(\frac{\max|r(t)|^2}{\max|y(t)|^2}\right), \tag{13}$$

where $r(t)$ is the reconstructed signal at the nonlinear port after time reversal as in Eq. (11) and $y(t)$ is the signal at the
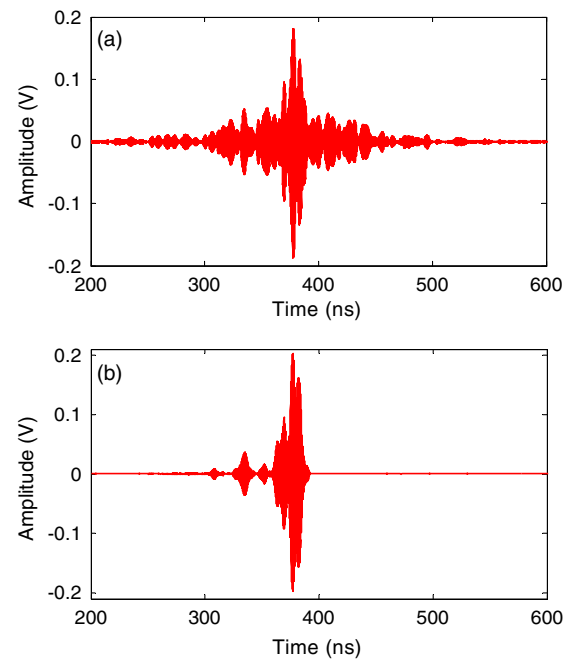
FIG. 4. (a) Reconstructed signal at the nonlinear port in the focusing stage compared with (b) the original excitation at the nonlinear port, plotted time reversed for better comparison.

nonlinear port after transmitting a simple pulse with the same peak amplitude at the input. The peak enhancement should be more prominent when the nonlinear excitation $g(t)$ is localized in time, since the reconstructed signal $r(t)$ will also be localized in time. This result makes PG an effective practical-performance metric of NLTR in a lossy complex environment where $g(t)$, consisting of a few short pulses, is localized in time [as opposed to the case in a highly reverberant system where $g(t)$ may not be localized in time].

For each discrete run with a new paddle position, nonlinear time reversal is applied, and the reconstructed signal at the nonlinear port is compared with the signals at the same port due to two different nondispersed pulses, i.e., short (10 ns) and long (200 ns) rectangular pulses. The peak gain values as defined in Eq. with respect to the responses to these short and long pulses, namely, PG_S and PG_L, are obtained. The short pulse is exactly the same pulse as the original interrogation pulse used for nonlinear time reversal. The second pulse is to resemble a narrowband continuous-wave-like signal. All waveforms are transmitted from port 2 at the peak input power level of 30 dBm. Figure 5 shows the signals at the nonlinear port that are (a) the reconstructed signal $r(t)$, using $s(t)$ from Fig. 3(c), (b) the signal due to the short pulse, $y_s(t)$, and (c) the signal due to the long pulse, $y_L(t)$. For both (b) and (c), the carrier frequency is $2f_0 = 3.5$ GHz. In the figure, the peak power of $r(t)$ is higher than that of both $y_s(t)$ and $y_L(t)$ with PG_S and PG_L of 11 and 5.5 dB, respectively, indicating a concentration of peak power at the nonlinear port via nonlinear time reversal.

$y_s(t)$ in Fig. 5(b) is the channel response (to a short pulse) between the nonlinear port and port 2, where the peak power is primarily determined by the direct or short orbit trajectories. The PG_S in essence is the measure of the temporal compression of a multipath spreading through time reversal and could vary depending on the scattering (multipath) condition of the enclosure.

The long pulse response $y_L(t)$ [Fig. 5(c)] is directly related to the steady-state mode of the enclosure, since the input signal is a narrowband single-tone pulse. The leveling
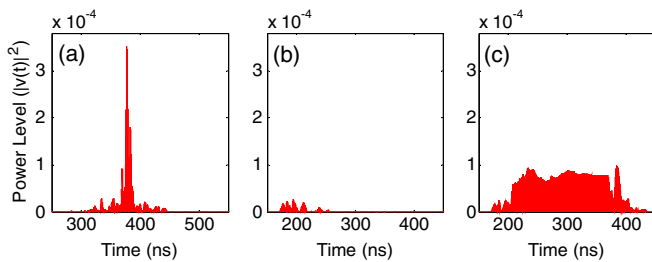
FIG. 5. Comparison of the signals at the nonlinear port: (a) reconstructed signal after NLTR, (b) signal due to nondispersive short (10-ns) pulse, and (c) signal due to nondispersive long (200-ns) pulse. For (b) and (c), the carrier frequency is $2f_0 = 3.5$ GHz.
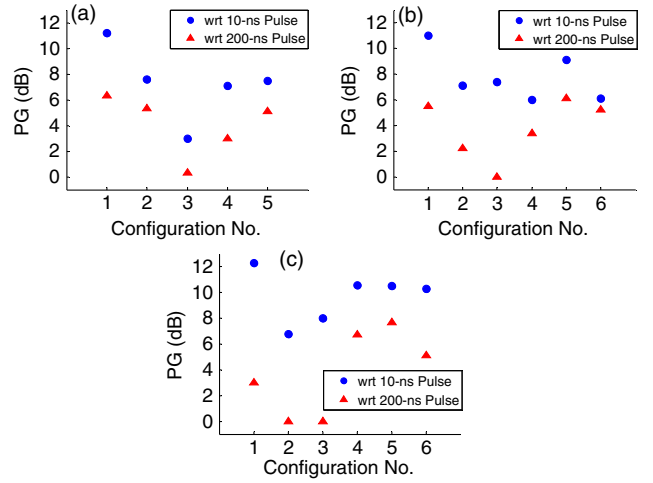
FIG. 6. Peak gain values obtained with various enclosure configurations for the interrogation pulse f_0 of (a) 1, (b) 1.5, and (c) 3.5 GHz (which means that the signals used for the PG calculation consists of $2f_0$).

of the amplitude in the later portion of the response indicates that the steady-state mode is established in the enclosure. Hence, the peak enhancement (PG_L) rather depends on the spatial mode of the enclosure at the corresponding frequency. In other words, the peak amplitude of $y_L(t)$ varies depending on whether the nonlinear port is positioned at a modal peak or null for a given configuration, which in turn varies the PG_L values.

Figure 6 presents the PG_S and PG_L values obtained for various enclosure configurations (paddle positions). The three plots in the figure correspond to the interrogation f_0 of (a) 1, (b) 1.75, and (c) 3.75 GHz, which means that the signals measured to obtain peak gain values consist of the corresponding $2f_0$. The PG_S values mostly stay above 6 dB (up to 12 dB), suggesting that, in general, good enhancement in peak power at the nonlinear port is achieved via nonlinear time reversal compared to sending a short non-TR pulse. The PG_L values are spread between 0 and 6 dB, which are generally lower than PG_S, due to the amplitude buildup to a steady state. The PG_L value of 0 dB implies that the nonlinear port is at a modal peak in the corresponding configuration, whereas the PG_L value of 6 dB points to a relative null. Therefore, sending in a long duration pulse could result in a "hit" or "miss," depending on the location of the nonlinear port. Furthermore, even for the hit case, there is no spatial concentration of peak power exclusively at the nonlinear port, since the modal peaks take place throughout the enclosure. Therefore, it shows that time reversal can be used to more efficiently concentrate peak power at a nonlinear port than both short and long simple pulses without TR.

IV. CONCLUSIONS

In this paper, we consider nonlinear electromagnetic time reversal applied to a lossy complex enclosure containing a

discrete passive nonlinear circuit. We also demonstrate the use of pulse inversion for extracting nonlinear responses, which could resolve practical issues of overlapping of linear and nonlinear spectral content and receiver linearity.

The utility of this approach as a means to efficiently concentrate peak power at the nonlinear element is demonstrated by comparing the signal peak amplitudes resulting from time reversal vs non-TR pulses. The results demonstrate good potential for practical application of nonlinear time reversal in complex propagation environments, particularly in the areas of wireless power transfer where NLTR can be used to efficiently transfer short pulses to power compact devices. By applying high-power amplification to NLTR signals, the focused pulse could also be used for applications such as microwave thermotherapy of cancer, as well as electronic disruption.

ACKNOWLEDGMENTS

[1] M. Fink, Time reversed acoustics, Phys. Today **50**, No. 3, 34 (1997).

[2] A. Parvulescu, Matched-signal ("MESS") processing by the ocean, J. Acoust. Soc. Am. **98**, 943 (1995).

[3] M. Fink, D. Cassereau, A. Derode, C. Prada, P. Roux, M. Tanter, J.-L. Thomas, and F. Wu, Time-reversed acoustics, Rep. Prog. Phys. **63**, 1933 (2000).

[4] G. Lerosey, J. de Rosny, A. Tourin, A. Derode, G. Montaldo, and M. Fink, Time reversal of electromagnetic waves, Phys. Rev. Lett. **92**, 193904 (2004).

[5] G. Lerosey, J. de Rosny, A. Tourin, and M. Fink, Focusing beyond the diffraction limit with far-field time reversal, Science **315**, 1120 (2007).

[6] S. M. Anlage, J. Rodgers, S. Hemmady, J. Hart, T. M. Antonsen, and E. Ott, New results in chaotic time-reversed electromagnetics: high frequency one-recording-channel time-reversal mirror, Acta Phys. Pol. A **112**, 569 (2007).

[7] A. Derode, A. Tourin, J. de Rosny, M Tanter, S. Yon, and M. Fink, Taking advantage of multiple scattering to communicate with time-reversal antennas, Phys. Rev. Lett. **90**, 014301 (2003).

[8] D. R. Jackson and D. R. Dowling, Phase conjugation in underwater acoustics, J. Acoust. Soc. Am. **89**, 171 (1991).

[9] D. Rouseff, D. R. Jackson, W. L. J. Fox, C. D. Jones, J. A. Ritcey, and D. R. Dowling, Underwater acoustic communication by passive-phase conjugation: Theory and experimental results, IEEE Journal of Oceanic Engineering **26**, 821 (2001).

[10] G. F. Edelmann, T. Akal, W. S. Hodgkiss, S. Kim, W. Kuperman, and H. C. Song, An initial demonstration of underwater acoustic communication using time reversal, IEEE Journal of Oceanic Engineering **27**, 602 (2002).

[11] H. W. Park, H. Sohn, K. H. Law, and C. R. Farrar, Time reversal active sensing for health monitoring of a composite plate, J. Sound Vib. **302**, 50 (2007).

[12] B. Taddese, J. Hart, T. Antonsen, E. Ott, and S. Anlage, Sensor based on extending the concept of fidelity to classical waves and overcoming the effects of dissipation, Appl. Phys. Lett. **95**, 114103 (2009); B. Taddese, T. Antonsen, E. Ott, and S. Anlage, Sensing small changes in a wave chaotic scattering system, J. Appl. Phys. **108**, 114911 (2010).

[13] C. Draeger and M. Fink, One-channel time reversal of elastic waves in a chaotic 2D-silicon cavity, Phys. Rev. Lett. **79**, 407 (1997).

[14] H. T. Nguyen, J. B. Andersen, and G. F. Pedersen, The potential use of time reversal techniques in multiple element antenna systems, IEEE Commun. Lett. **9**, 40 (2005).

[15] I. Naqvi, G. El Zein, G. Lerosy, J. de Rosny, P. Besnier, A. Tourin, and M. Fink, Experimental validation of time reversal ultra wide-band communication system for high data rates, IET Microwaves Antennas Prop. **4**, 643 (2010).

[16] H. El-Sallabi, P. Kyritsi, A. Paulraj, and G. Papanicolaou, Experimental investigation on time reversal precoding for space-time focusing in wireless communications, IEEE Trans. Instrum. Meas. **59**, 1537 (2010).

[17] A. Dezfooliyan and A. M. Weiner, Experimental investigation of UWB impulse response and time reversal technique up to 12 GHz: Omnidirectional and directional antennas, IEEE Trans. Antennas Propag. **60**, 3407 (2012).

[18] B. Wang, Y. Wu, F. Han, Y.-H. Yang, and K. J. R. Liu, Green wireless communications: A time-reversal paradigm, IEEE J. Sel. Area Commun. **29**, 1698 (2011); F. Han, Y.-H. Yang, B. Wang, Y. Wu, and K. J. R. Liu, Time-reversal division multiple access over multi-path channels, IEEE Trans. Commun. **60**, 1953 (2012); Y. Chen, Y.-H. Yang, F. Han, and K. J. R. Liu, Time-reversal wideband communications, IEEE Signal Process. Lett. **20**, 1219 (2013).

[19] R. Kosmas and C. M. Rappaport, Time reversal with the FDTD method for microwave breast cancer detection, IEEE Trans. Microwave Theory Tech. **53**, 2317 (2005).

[20] M. E. Yavuz and F. L. Teixeira, Space-frequency ultrawide-band time-reversal imaging, IEEE Trans. Geosci. Remote Sens. **46**, 1115 (2008).

[21] M. Fink, G. Montaldo, and M Tanter, Time-reversal acousticcs in biomedical engineering, Annu. Rev. Biomed. Eng. **5**, 465 (2003).

[22] F. Lemoult, M. Fink, and G. Lerosey, Acoustic resonators for far-field control of sound on a subwavelength scale, Phys. Rev. Lett. **107**, 064301 (2011).

[23] Y. Jin, J. Moura, and N. O'Donoughue, Time reversal multiple-input multiple-output radar, IEEE J. Select. Top. Signal Process. **4**, 210 (2010).

[24] F. Foroozan and A. Asif, Time reversal based active array source localization, IEEE Trans. Signal Process. **59**, 2655 (2011).

[25] D. Zhao, Y. Jin, B.-Z. Wang, and R. Zang, Time reversal based broadband synthesis method for arbitrary structured beam-steering arrays, IEEE Trans. Antennas Propag. **60**, 164 (2012).

[26] M. Davy, J. de Rosny, J-.C. Joly, and M. Fink, Focusing and amplification of electromagnetic waves by time reversal in a leaky reverberation chamber, C.R. Phys. **11**, 37 (2010).

[27] D. Carsenat and C. Decroze, UWB antennas beamforming using passive time-reversal device, IEEE Antennas Wireless Propag. Lett. **11**, 779 (2012).

[28] S. K. Hong, B. T. Taddese, Z. D. Drikas, S. M. Anlage, and T. D. Andreadis, Focusing an arbitrary pulse at a distance using time-reversal techniques, J. Electromagn. Waves Appl. **27**, 1262 (2013); S. K. Hong, V. M. Mendez, W. S. Wall, and R. Liao, Single-feed beam-steering of short pulses via time reversal, IEEE Antennas Wireless Propag. Lett. **13**, 794 (2014).

[29] B. T. Taddese, G. Gradoni, F. Mogile, T. M. Antonsen, E. Ott, and S. M. Anlage, Quantifying volume changing perturbations in a wave chaotic system, New J. Phys. **15**, 023025 (2013); B. T. Taddese, T. M. Antonsen, E. Ott, and S. M. Anlage, The effects of non-uniform loss on time reversal mirrors, AIP Adv. (to be published).

[30] M. Frazier, B. Taddese, T. Antonsen, and S. M. Anlage, Nonlinear time reversal in a wave chaotic system, Phys. Rev. Lett. **110**, 063902 (2013); M. Frazier, B. Taddese, B. Xiao, T. Antonsen, E. Ott, and S. M. Anlage, Nonlinear time reversal of classical waves: experiment and model, Phys. Rev. E **88**, 062910 (2013).

[31] S. D. Cohen, H. L. D. de S. Cavalcante, and D. J. Gauthier, Subwavelength position sensing using nonlinear feedback and wave chaos, Phys. Rev. Lett. **107**, 254103 (2011).

[32] M. Scalerandi, A. S. Gliozzi, C. L. E. Bruno, and K. Van Abeele, Nonlinear acoustic time reversal imaging using the scaling subtraction method, J. Phys. D **41**, 215404 (2008).

[33] T. J. Ulrich, P. A. Johnson, and A. Sutin, Imaging nonlinear scatterers applying the time reversal mirror, J. Acoust. Soc. Am. **119**, 1514 (2006).

[34] C.-L. Hsieh, Y. Pu, R. Grange, and D. Psaltis, Digital phase conjugation of second harmonic radiation emitted by nanoparticles in turbid media, Opt. Express **18**, 12283 (2010).

[35] D. H. Simpson, C. T. Chin, and P. N. Burns, Pulse inversion Doppler: A new method for detecting nonlinear echoes from microbubble contrast agents, IEEE Trans. Ultrason. Ferroelectr. Freq. Control **46**, 372 (1999).

[36] See Supplemental Material at http://link.aps.org/supplemental/10.1103/PhysRevApplied.2.044013 for the loss comparison between a closed and open cavity, as well as the demonstration of spatial focusing from NLTR using a numerical simulation of a two-dimensional model of the experimental cavity.

[37] Frequency doublers used for the experiment are Mini-Circuits® ZX90 − 2 − 11 − S+, ZX90 − 2 − 19 − S+, and ZX90 − 2 − 50 − S+.

[38] P. N. T. Wells, Ultrasound imaging, Phys. Med. Biol. **51**, R83 (2006).